J Mater Sci (2007) 42:9221–9226
DOI 10.1007/s10853-007-1905-2

Synthesis and characterization of $LiNi_{0.9}Co_{0.1}O_2$ for lithium batteries

Daocong Li · Zhenghe Peng · Wenyong Guo · Chaoqun Yuan · Yangmei Liu · Yunhong Zhou

Received: 10 November 2006 / Accepted: 31 May 2007 / Published online: 27 July 2007

Abstract $LiNi_{0.9}Co_{0.1}O_2$ cathode material is prepared from $LiOH{\cdot}H_2O$ and $Ni_{0.9}Co_{0.1}(OH)_2$ by co-precipitation and subsequent two-stage heat treatment in flowing oxygen based on the results of thermogravimetric. The structural and electrochemical properties of the samples are characterized by means of inductively coupled plasma-atomic emission spectrometer (ICP-AES), X-ray diffraction (XRD), scanning electron microscope (SEM), cyclic voltammogram (CV) and charge–discharge studies. All the samples sintered at different temperatures have a typical layered structure with space group *R3-m* and good electrochemical performances. The sintering temperature has a remarkable effect on the electrochemical performance of the samples. The sample sintered at 730 °C shows the largest initial discharge capacity 191.1 mAh g^{-1} (50 mA g^{-1}, 3.0–4.3 V) and the best cycling performance. The initial discharge capacity rises to above 200 mAh g^{-1} with the voltage range 3.0–4.5 V.

Introduction

Lithium cobalt oxide ($LiCoO_2$) has been used as a cathode material in the majority of commercial lithium batteries due to its excellent electrochemical properties, such as high output voltage, long life cycle, and easy preparation [1–3]. However, the high cost and toxicity of this material have led to the intensive investigations on the possible alternatives during the last decade. Lithium nickel oxide ($LiNiO_2$) has been considered as a promising cathode material due to its low cost and high specific energy. Nevertheless, it is very difficult to synthesize a stoichiometric $LiNiO_2$ [4, 5]. The non-stoichiometry material has a poor cycling performance because excess nickel ions are located in the lithium plane, hindering the diffusion of lithium during electrochemical cycling [6–8]. Therefore, iso-structural solid solutions of $LiNi_{1-x}Co_xO_2$ have been studied for their electrochemical properties. Julien et al. [9] prepared $LiNi_{0.3}Co_{0.7}O_2$ using a mixture of citric acid and glycine. Belharouak et al. [10] used a precipitation method to synthesize $LiNi_{0.5}Co_{0.5}O_2$. Cho et al. [11] obtained a spherulitic $Ni_{0.74}Co_{0.26}(OH)_2$ by a co-precipitation method, and reacted it with $LiOH{\cdot}H_2O$ at 750 °C to produce well-defined spherical particles of $LiNi_{0.74}Co_{0.26}O_2$. Fey et al. reported the sol-gel synthesis of $LiNi_{0.8}Co_{0.2}O_2$ using maleic acid [12] and a series of saturated aliphatic dicarboxylic acids [13] as a chelating agent. Oh et al. [14] used an acid dissolution method to produce $LiNi_{0.8}Co_{0.2}O_2$. Wu et al. [15] prepared $LiNi_{0.8}Co_{0.2}O_2$ used a precipitation method. Within this system, $LiNi_{0.8}Co_{0.2}O_2$ has been given much attention as a possible cathode material. The raw materials and synthesis processes, especially the heat treatment process, have a significant effect on the electrochemical performance of $LiNi_{1-x}Co_xO_2$ material. The studies of $LiNi_{0.9}Co_{0.1}O_2$ are relatively lesser comparing with $LiNi_{0.8}Co_{0.2}O_2$. Several studies show that the reversible discharge capacity of $LiNi_{0.9}Co_{0.1}O_2$ is less than 150 mAh g^{-1} [16–18]. In order to improve the reversible capacity of $LiNi_{0.9}Co_{0.1}O_2$, we adopt a novel method consisting of co-precipitation and two-stage heat treatment to synthesize $LiNi_{0.9}Co_{0.1}O_2$ compounds. We optimize the synthesis conditions and

D. Li · Z. Peng (✉) · W. Guo · C. Yuan · Y. Liu · Y. Zhou
Department of Chemistry, Wuhan University, Wuhan 430072, P.R. China
e-mail: zhhpeng@126.com

examine the relationship between the synthesis conditions and the electrochemical properties.

Experimental

The precursor $Ni_{0.9}Co_{0.1}(OH)_2$ was prepared by the co-precipitation method. About 1 M aqueous solution of nickel and cobalt nitrates was prepared according to the above molar ratio. The solution of $LiOH{\cdot}H_2O$ was slowly added with stirring and the pH was controlled between 11 and 12. The obtained hydroxide mixture was filtered and thoroughly washed with distilled water until the pH = 7 and dried at 120 °C for 24 h. The dried hydroxide was then grounded with an excess of $LiOH{\cdot}H_2O$ (Li/(Ni + Co) = 1.05). Excess lithium compensates for lithium vaporization at high temperature. Thermal decomposition behavior of the mixed precursor was examined by thermogravimetric and differential thermal analysis (TG/DTA, NETZSCH STA 449C) in static air at a heating rate of 10 °C min^{-1}. Based on the results of TG/DTA, the heat treatment temperatures were chosen. The mixed powders were preheated at 600 °C for 8 h. After grinding, the materials were sintered at 700, 730, 760, and 800 °C for 20 h in flowing oxygen, respectively.

The crystalline structure of the prepared powder was investigated by means of powder X-ray diffraction (XRD, SHIMADZU, XRD-6000) using Cu Kα radiation. The powder morphology was observed by a scanning electron microscope (SEM, HITACHI, X-650). The Li, Ni, and Co contents of the synthesized material were analyzed using an inductively coupled plasma-atomic emission spectrometer (ICP-AES, Thermo Electron, IRIR Intrepid II XSP).

The electrochemical cycling performance of the material was studied by assembling model test cells. Test cathode electrodes were prepared by mix 80:15:5 (mass ratio) of active material, acetylene black, and PTFE binder, respectively, in isopropyl alcohol. After rolling the mixture to be a membrane, a circular disc of 0.8 cm in diameter from the membrane was cut out and pressed onto stainless steel mesh to become a current collector, and then dried at 120 °C in a vacuum furnace for 12 h. The model test cells were assembled using lithium foil as an anode and 1 M $LiClO_4$ in 1:1 (volume ratio) ethylene carbonate (EC) and dimethyl carbonate (DMC) as an electrolyte and Celgard 2300 membrane as separator in an argon-filled glove box. The charge–discharge cycles were carried out at room temperature and a constant current density of 20, 50, 100, and 200 mA g^{-1} with cut-off voltage of 3.0 to 4.3 and 4.5 V, respectively. Cyclic voltammogram was run on a CHI 604C electrochemical workstation at a scan rate of 0.1 mV s^{-1} from 2.5 to 4.5 V versus Li/Li^+ with lithium foil as reference and counter electrodes.

Results and discussions

Thermal analysis

The TG/DTA curves for the mixed precursor are shown in Fig. 1. The TG curve shows that weight loss takes place in several steps. The first weight loss step between room temperature to 150 °C is attributed to the removal of crystal water of $LiOH{\cdot}H_2O$ with 16% weight loss, which is associated with the sharp endothermic peak at 97 °C in DTA curve. The second step of 12% weight loss, which occurs between 150 and 400 °C, is attributed to the decomposition of $Ni_{0.9}Co_{0.1}(OH)_2$, corresponding to a endothermic peak at 240 °C in DTA curve. The third step of 1% weight loss between 400 and 600 °C is attributed to the decomposition of LiOH. Around 600 °C, the active reaction takes place and the precursor starts to form the compound. In the temperature range of higher than 700 °C, there is a continuous weight loss process, which is attributed to part decomposition of the as-formed crystalline because of the loss of oxygen and lithium [19, 20], resulting in non-stoichiometric compounds $Li_{1-x}Ni_{0.9}Co_{0.1}O_{2-y}$. Therefore, we choose two-stage heating treatment at 600 °C for 8 h and after grinding, sintering at higher temperature for 20 h in flowing oxygen.

ICP, XRD and SEM studies

The ICP-AES analysis for $LiNi_{0.9}Co_{0.1}O_2$ at various sintering temperatures is summarized in Table 1. As the temperature rises, the lithium content becomes slight lower due to the volatilization of lithium. The results are in agreement with the calculated compositions during synthesis within the limits of error.

The XRD patterns of the $LiNi_{0.9}Co_{0.1}O_2$ powders prepared at various sintering temperatures for 20 h are shown in Fig. 2. The patterns show that all the samples

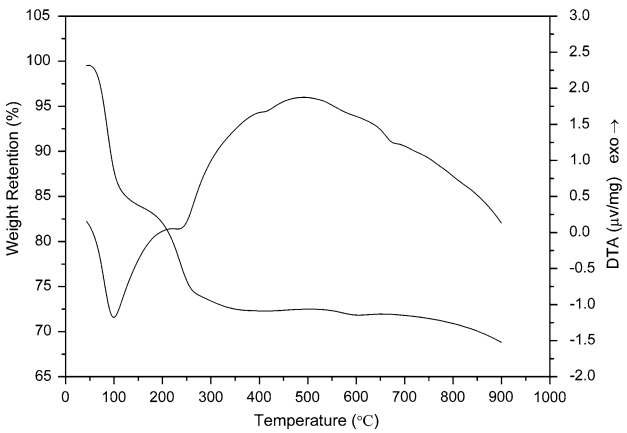

Fig. 1 TG/DTA curves for $LiNi_{0.9}Co_{0.1}O_2$ precursor

Table 1 The compositions of $LiNi_{0.9}Co_{0.1}O_2$ powders prepared at various sintering temperatures

Composition	Li	Ni	Co
700 °C	1.029	0.892	0.108
730 °C	1.011	0.895	0.105
760 °C	0.982	0.894	0.106
800 °C	0.973	0.896	0.104

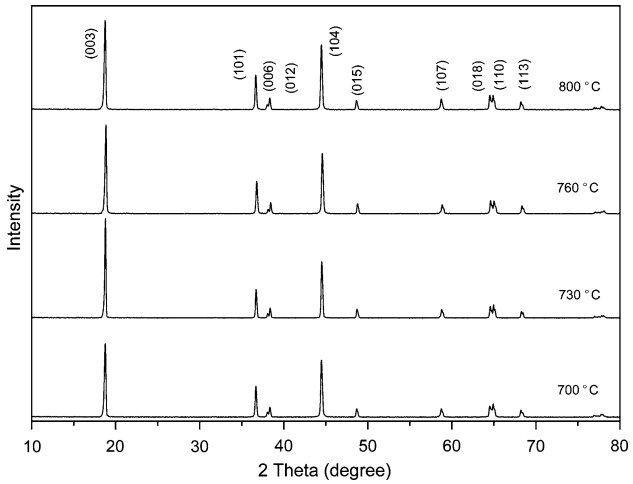

Fig. 2 The XRD patterns of $LiNi_{0.9}Co_{0.1}O_2$ powders prepared at various sintering temperatures

have a typical layered structure with space group *R3-m*, in which the O^{2-} ions form a closely-packed, face-centered-cubic structure, in which the Ni^{3+} and Co^{3+} ions occupy the crystallographically equivalent of 3b sites and Li^+ ion occupy the 3a sites. All the XRD patterns have sharp peaks and display the hexagonal doublets (006)/(102) and (108)/(110) with a clear splitting, which indicate a high degree of crystallinity and good hexagonal ordering [21]. The variation of lattice parameters (*a* and *c*), *c*/*a* ratio, $I_{(003)}/I_{(104)}$ ratio, *R*-factor $[(I_{(006)} + I_{(102)})/I_{(101)}]$ and unit-cell volume of the $LiNi_{0.9}Co_{0.1}O_2$ powders sintered at different temperatures is summarized in Table 2. There are no significant change in the parameter values of *a*, *c*, *c*/*a* for the samples sintered at different temperatures. A relatively large increase in the $I_{(003)}/I_{(104)}$ ratio is observed for the sample sintered at 730 °C. According to Gao et al. [22], an increase in the $I_{(003)}/I_{(104)}$ ratio indicates that the sample has good cation ordering. The good cation ordering is also evident from the well-separated (108) and (110) reflections [23, 24]. According to Riemers et al. [25], the *R*-factor, defined as the ratio of the intensities of the hexagonal characteristic doublet peaks (006) and (102) to the (101) peak, is utilized to estimate the hexagonal ordering. The lower the *R*-factor is, the better the hexagonal ordering is. The *R*-factors of all the samples are low and the sample sintered at 730 °C has the lower *R*-factors, which indicates the better hexagonal ordering. Moreover, Dahn et al. [26] reported that material with more layered characteristics would have lower cell volume. The unit-cell volume for the sample sintered at 730 °C is smaller than the samples sintered at other temperatures. Hence, the sample sintered at 730 °C has more layered characteristics than other samples. Therefore, the $LiNi_{0.9}Co_{0.1}O_2$ sample sintered at 730 °C has the better cation ordering, better hexagonal ordering and more layered characteristics than other samples and can has the better electrochemical performance.

The SEM photographs of $LiNi_{0.9}Co_{0.1}O_2$ sample sintered at 730 °C with different multiple (5 and 10 k) are shown in Fig. 3. The sample has the homogeneous distribution of the particles with sub-micron size. The intercalation process of Li^+ ion between the layers of the cathode is a diffusion process. Therefore, the smaller particles, which will lead to a short path for Li^+ ions, are favorable to intercalation and the sample is expected to deliver a good electrochemical performance.

Electrochemical properties

The electrochemical properties of $LiNi_{0.9}Co_{0.1}O_2$ at various sintering temperatures are examined. The charge–discharge studies are carried out at room temperature and a constant current density of 50 mA g^{-1} with cut-off voltage of 3.0–4.3 V for up to 20 cycles. The cycling performances of the samples are shown in Fig. 4. The initial specific discharge capacities are 173.0, 191.1, 183.2, and 168.1 mAh g^{-1} for samples sintered at 700, 730, 760, and 800 °C, respectively, and reversible specific discharge capacities after 20 cycles are 154.9, 178.6, 164.6, and 151.4 mAh g^{-1}. The capacity retentions after 20 cycles are similar and the value 93.5% at 730 °C is relatively larger.

Table 2 Lattice parameters, *c*/*a* values, $I_{(003)}/I_{(104)}$ intensity ratio, *R*-factor and unit-cell volume of $LiNi_{0.9}Co_{0.1}O_2$ powders prepared at various sintering temperatures

Temperature (°C)	*a* (Å)	*c* (Å)	*c*/*a* ratio	$I_{(003)}/I_{(104)}$	*R*-factor $[(I_{(006)} + I_{(102)})/I_{(101)}]$	Unit-cell volume (Å^3)
700	2.871	14.177	4.938	1.04	0.480	101.17
730	2.862	14.148	4.943	1.41	0.463	100.36
760	2.866	14.153	4.938	1.20	0.479	100.65
800	2.871	14.181	4.939	1.14	0.469	101.22

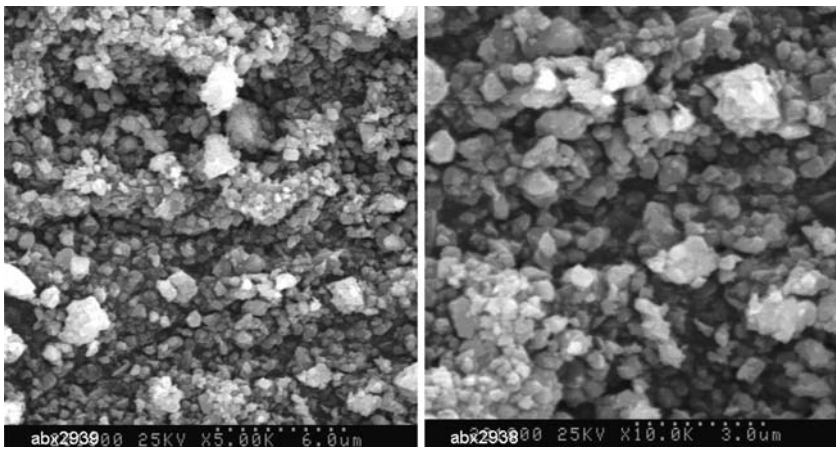

Fig. 3 SEM photographs of $LiNi_{0.9}Co_{0.1}O_2$ powders prepared at 730 °C

The sintering temperature has an obvious effect on the initial specific discharge capacity. When the sintering temperature is increased from 700 to 730 °C, the initial specific discharge capacity increases to 191.1 mAh g^{-1} and when the sintering temperature is increased to 760 and 800 °C, the initial specific discharge capacity decreases to183.2 and 168.1 mAh g^{-1}, respectively. Among the $LiNi_{0.9}Co_{0.1}O_2$ samples at various sintering temperatures for 20 h, the sample sintered at 730 °C shows highest reversible discharge capacity. As indicate by the results of XRD studies, the system becomes more layered at 730 °C and the 3a lithium and 3b transition metal ion sites become ordered, facilitating the intercalation-deintercalation process [27]. The decrease in electrochemical performance of the material sintered at 800 °C is mainly attributed to the loss of lithium by volatilization due to the higher temperature, which is proved by the ICP-AES results. The structure studies indicate a decrease in cation ordering and layered characteristics when the sintered temperature is increased to 800 °C.

From electrochemical result of the sample sintered at 730 °C, shown in Fig. 5, it is found that there are distinct plateaux in the charge–discharge curves. The plateaux correspond to structural changes in the charge–discharge process, a phase transition between a monoclinic phase and a hexagonal phase and a transition between a hexagonal phase and another hexagonal phase, which is a unique characteristic of $LiNi_{1-x}Co_xO_2$ compounds [28–30]. Cyclic voltammogram for the sample sintered at 730 °C is shown in Fig. 6. In the first cycle, the major anodic peak is observed at 4.02 V and the minor peak at 4.22 V that correspond to the delithiation from the lattice. The cathodic minor peaks are centered at 4.09, 3.94 V and the major peak at 3.65 V, which corresponds to the intercalcation of the Li ion. In the second cycle, the major anodic peak is centered at 3.84 V, which has a large shift to lower potential, but the corresponding cathodic peak remains with a slight shift of 0.01 V to higher potential. The initial shift in the first cycle anodic peak potential is an indication of the electrochemical alteration in the active materials,

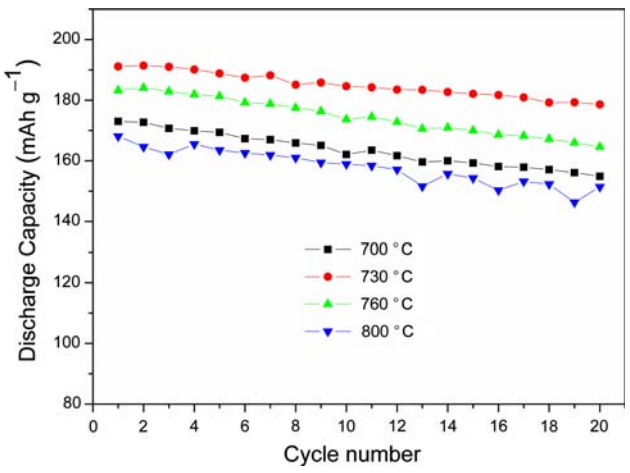

Fig. 4 Discharge capacity as function of cycle number for $LiNi_{0.9}Co_{0.1}O_2$ samples prepared at various sintering temperatures (50 mA g^{-1}, 3.0–4.3 V)

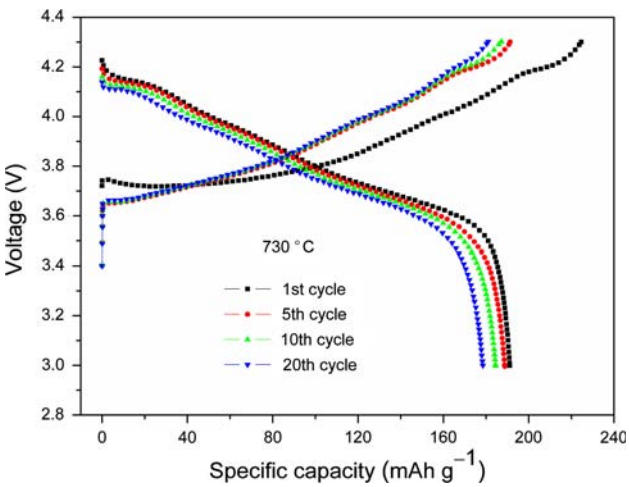

Fig. 5 Voltage vs. capacity curves for the $LiNi_{0.9}Co_{0.1}O_2$ sample prepared at 730 °C (50 mA g^{-1}, 3.0–4.3 V)

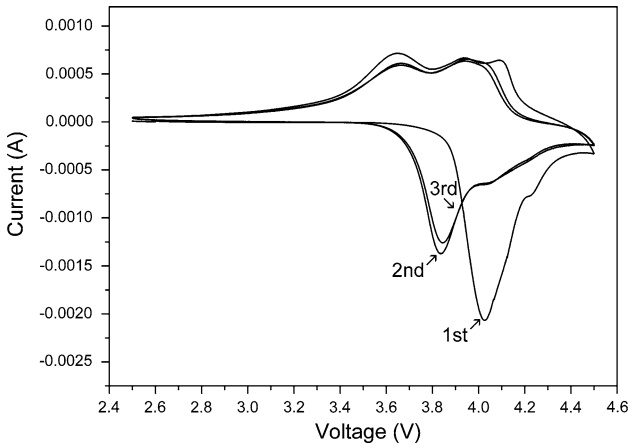

Fig. 6 Cyclic voltammogram at a scan rate of 0.1 mV s^{-1} from 2.5 to 4.5 V for the $LiNi_{0.9}Co_{0.1}O_2$ sample prepared at 730 °C

which allow for better electrical contact with the conducting carbon particles, liquid electrolyte and current-collector of the electrode. Further cycles show minor shifts in the anodic and cathodic peak potentials, which indicate reversibility of the charge–discharge reaction. The peak potentials remain almost constant, but the relative peak intensities and area under the peak decrease with cycle number, which correspond to capacity fade. The minor peaks associated with phase transitions are agree with the plateaux in the charge–discharge curves, which debase the cycle stability of materials and cause capacity fade [29].

The Fig. 7 shows the specific discharge capacities of the sample sintered at 730 °C at different current density (20, 50, 100, and 200 mA g^{-1}) and different voltage range (3.0–4.3 and 4.5 V). When the voltage range is 3.0–4.3 V, the specific discharge capacities at first cycle are 202.4, 191.1, 183.5, and 172.1 mAh g^{-1}, while capacity rentions after 20 cycles are 91.1, 93.5, 95.6, and 97.7% for current density 20, 50, 100, and 200 mA g^{-1}, respectively. When the cut-off voltage is 4.5 V, the specific discharge capacities at first cycle are 214.2, 203.7, 197.2, and 188.9 mAh g^{-1}, and capacity rentions after 20 cycles are 76.5, 85.7, 89.4, and 91.7% for current density 20, 50, 100, and 200 mA g^{-1}, respectively. Along with the current density increasing, the initial specific discharge capacity decreases, but the cycle performance increases. As the charging cut-off voltage increases from 4.3 to 4.5 V, the initial specific discharge capacity increases to above 200 mAh g^{-1}, however, the capacity rention decreases markedly. When the charging cut-off voltage increases and charge–discharge current density decreases, the deeper lithium extraction may cause the greater change in the structure of material and result in the reduction of the cycling stability [31]. In addition, the electrochemical properties of sample prepared by our method are better than those prepared by sol-gel method [16, 17] and combustion method [18].

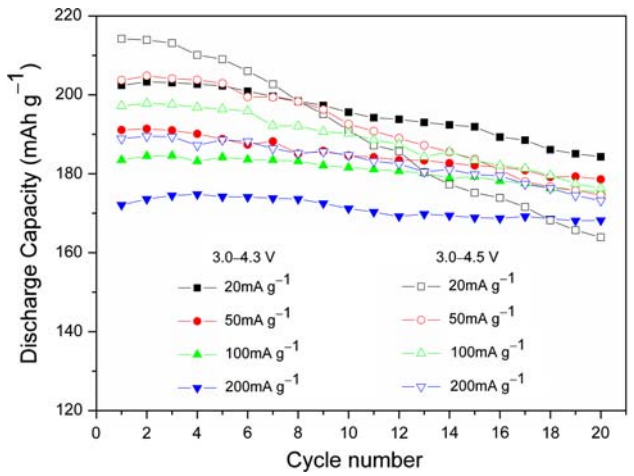

Fig. 7 Discharge capacity as function of cycle number for $LiNi_{0.9}Co_{0.1}O_2$ sample prepared at 730 °C with voltage range of 3.0–4.3 and 4.5 V, at current density of 20, 50, 100, and 200 mA g^{-1}, respectively

Conclusions

$LiNi_{0.9}Co_{0.1}O_2$ cathode material was prepared by co-precipitation and subsequently two-stage heat treatment. All the samples sintered at different temperatures have a two-dimensional layered structure, as confirmed by XRD results. The sintering temperature has a significant effect on the electrochemical performance of the samples. The sample sintered at 730 °C for 20 h has the largest initial discharge capacity 191.1 mAh g^{-1} (50 mA g^{-1}, 3.0–4.3 V) and shows the best electrochemical performance, capacity rention after 20 cycles is 93.5%. This is due to good cation ordering, hexagonal ordering and crystallinity, as well as relatively small and uniform particle size. When the cut-off voltage increases to 4.5 V, the initial discharge capacity rises to above 200 mAh g^{-1}. Although the cycling stability is contrary proportional to the upper limit voltage, it is possible to improve the reversibility in high upper limit voltage by surface coating technology further [32, 33]. Therefore, we think that $LiNi_{0.9}Co_{0.1}O_2$ cathode material synthesized by our method can be a promising cathode material for lithium batteries.

Acknowledgments We gratefully acknowledge the financial support from the National Nature Science Foundation of China (No. 29833090 and No. 29771025).

References

1. Nagaura T, Taza K (1990) Prog Batt Sol Cells 9:20
2. Fu LJ, Liu H, Li C, Wu YP, Rahm E, Holze R, Wu HQ (2005) Prog Mater Sci 50:881

3. Wu YP, Rahm E, Holze R (2002) Electrochim Acta 47:3491
4. Morales J, Perez C, Tirado JL (1990) Mater Res Bull 25:623
5. Ohzuku T, Ueda A (1994) Solid State Ionics 69:201
6. Arai H, Okada S, Ohtsuka H, Ichimura M (1995) Solid State Ionics, 80:261
7. Dokko K, Nishizawa M, Horikoshi S, Itoh T, Mohamed M, Uchida I (2000) Electrochem Solid state Lett 3:125
8. Broussely M, Biensan P, Simon B (1999) Electrochim Acta 45:3
9. Julien C, Michael SS, Ziolkiewicz S (1999) Int J Inorg Mater 1:29
10. Belharouak I, Tsukamoto H, Amine K (2003) J Power Sources 119–121:175
11. Cho J, Park B (2001) J Power Sources 92:35
12. Fey GTK, Shiu RF, Subramanian V, Chen JG, Chen CL (2002) J Power Sources 103:265
13. Fey GTK, Chen JG, Wang ZF, Yang HZ, Kumar TP (2004) Mater Chem Phys 87:246
14. Oh SH, Jeong WT, Cho WI, Cho BW, Woo K (2005) J Power Sources 140:145
15. Wu S, Yang CW (2005) J Power Sources 146:270
16. Fey GTK, Shiu RF, Kumar TP, Chen CL (2003) Mater Sci Eng B 100:234
17. Hwang BJ, Santhannam R, Chen CH (2003) J Power Sources 114:244
18. Song M, Kwon I, Kim H (2005) J Appl Electrochem 35:1073
19. Wang GX, Zhong S, Bradhurst DH, Dou SX, Liu HK (1998) J Power Sources 76:141
20. Li W, Currie JC (1997) J Electrochem Soc 144:2773
21. Fey GTK, Wang ZF, Kumar TP (2002) Ionics 8:351
22. Gao Y, Yakovieva MV, Ebner WB (1998) Electrochem Solid State Lett 1:117
23. Kim J, Fulmer P, Manthiram A (1999) Mater Res Bull 34:571
24. Gummow RJ, Thackeray MM, David WIF, Hull S (1992) Mater Res Bull 27:327
25. Reimers JR, Rossen E, Jones CD, Dahn JR (1993) Solid State Ionics 61:335
26. Dahn JR, Von Sacken U, Michal CA (1990) Solid State Ionics 44:87
27. Gover RKB, Kanno R, Mitchell BJ, Yonemura M, Kawamoto Y (2000) J Electrochem Soc 147:4045
28. Li W, Reimers JN, Dahn JR (1993) Solid State Ionics 67:123
29. Cho J, Jung H, Park Y, Kim G, Lim H (2000) J Electrochem Soc 147:15
30. Wang GX, Lindsay MJ, Ionescu M, Bradhurst DH, Dou SX, Liu HK (2001) J Power Sources 97–98:298
31. Chebiam RV, Prado F, Manthiram A (2001) Chem Mater 13:2951
32. Omanda H, Brousse T, Marhic C, Schleich DM (2004) J Electrochem Soc 151:A992
33. Cho J, Kim TJ, Noh M, Park B (2004) J Electrochem Soc 151:A1889